

# Engineering Substrate Interactions for High Luminescence Efficiency of Transition-Metal Dichalcogenide Monolayers

Yifei Yu, Yiling Yu, Chao Xu, Yong-Qing Cai, Liqin Su, Yong Zhang, Yong-Wei Zhang,\* Kenan Gundogdu,\* and Linyou Cao\*

It is demonstrated that the luminescence efficiency of monolayers composed of MoS<sub>2</sub>, WS<sub>2</sub>, and WSe<sub>2</sub> is significantly limited by the substrate and can be improved by orders of magnitude through substrate engineering. The substrate affects the efficiency mainly through doping the monolayers and facilitating defect-assisted nonradiative exciton recombinations, while the other substrate effects including straining and dielectric screening play minor roles. The doping may come from the substrate and substrate-borne water moisture, the latter of which is much stronger than the former for MoS<sub>2</sub> and WS<sub>2</sub> but negligible for WSe<sub>2</sub>. Using proper substrates such as mica or hexagonal boron nitride can substantially mitigate the doping effect. The defect-assisted recombination depends on the interaction between the defect in the monolayer and the substrate. Suspended monolayers, in which the substrate effects are eliminated, may have efficiency up to 40% at room temperatures. The result provides useful guidance for the rational design of atomic-scale light emission devices.

## 1. Introduction

2D transition metal dichalcogenide (TMDC) materials such as monolayer MoS<sub>2</sub>, WS<sub>2</sub>, and WSe<sub>2</sub> promise to enable the development of atomic-scale light emission devices, but their luminescence efficiencies have been shown to be surprisingly low despite the materials' perfect surface passivation and strong exciton binding energy.<sup>[1]</sup> Recent studies indicate that the optical properties of 2D TMDC materials are susceptible to

Y. Yu, Prof. L. Cao  
Department of Materials Science and Engineering  
North Carolina State University  
Raleigh, NC 27695, USA  
E-mail: lcao2@ncsu.edu

Y. Yu, C. Xu, Prof. K. Gundogdu, Prof. L. Cao  
Department of Physics  
North Carolina State University  
Raleigh, NC 27695, USA  
E-mail: kgundog@ncsu.edu

Dr. Y.-Q. Cai, Dr. Y.-W. Zhang  
Institute of High Performance Computing  
A\*STAR, Singapore 138632  
E-mail: zhangyw@ihpc.a-star.edu.sg

L. Su, Prof. Y. Zhang  
Department of Electrical and Computer Engineering  
The University of North Carolina at Charlotte  
Charlotte, NC 28223, USA

DOI: 10.1002/adfm.201600418



the influence of substrates.<sup>[2]</sup> It has been reported that substrates may affect the luminescence efficiency of the monolayers by inducing strain, doping, or dielectric screening.<sup>[2a,e-g,3]</sup> However, despite the recent progress, many important questions about the substrate effect have remained to be answered. For instance, while it is known that substrates could affect the luminescence efficiency through multiple ways, there is no quantitative understanding for the effect of each mechanism and no knowledge on which mechanism could be dominant. More importantly, it is not clear how the effect of substrates might depend on the nature of the substrate and the physical features of the monolayers. Answers to these questions would provide useful guidance for the realization of optimal luminescence efficiency through engineering the substrate effects.

Here we quantitatively evaluate the effect of substrates on the luminescence efficiency of monolayers MoS<sub>2</sub>, WS<sub>2</sub>, and WSe<sub>2</sub> and demonstrate strategies of substrate engineering to improve the efficiency by orders of magnitude. We find that the main effects of the substrate lie in doping the monolayers and facilitating defect-assisted nonradiative exciton recombinations. The doping may be from substrate-borne water moisture and the substrate itself, the former of which is much stronger than the latter for WS<sub>2</sub> and MoS<sub>2</sub> but negligible for WSe<sub>2</sub>. Using proper substrates can substantially mitigate the doping effect on the photoluminescence (PL), such as mica for WS<sub>2</sub> and MoS<sub>2</sub> and hexagonal boron nitride (h-BN) or polystyrene (PS) for WSe<sub>2</sub>. The defect-assisted recombination depends on the interaction of the defects in the monolayer such as sulfur vacancies with the substrate and may be substantially suppressed by either removing the substrate or lowering the number of defects. In this work we largely ignore the optical resonance effects associated with the substrate's geometrical features.<sup>[4]</sup>

## 2. Results and Discussion

We start with comparing the PL of suspended MoS<sub>2</sub>, WS<sub>2</sub>, and WSe<sub>2</sub> monolayers to those of as-grown counterparts. The monolayers were synthesized on sapphire substrates using chemical vapor deposition (CVD) processes as described previously,<sup>[5]</sup> and the suspended monolayers were prepared by manually

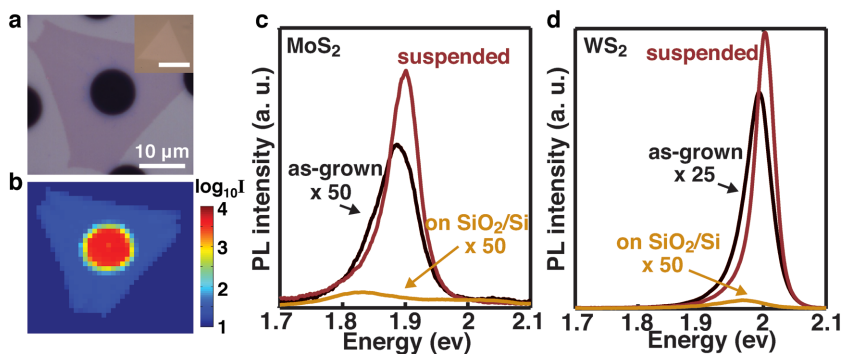


**Figure 1.** Improved luminescence efficiency of suspended monolayers. a) Optical image of a typical suspended monolayer. Inset: an as-grown monolayer (scale bar: 10  $\mu\text{m}$ ). b) Photoluminescence (PL) mapping of the suspended monolayer. The color bar of PL intensity is in logarithm scale. c) PL spectra of as-grown monolayer  $\text{MoS}_2$  on sapphire substrates, suspended monolayer  $\text{MoS}_2$ , and the monolayer  $\text{MoS}_2$  transferred onto  $\text{SiO}_2/\text{Si}$  substrates with 300 nm thick thermally grown oxide. The spectra of the as-grown and the one on  $\text{SiO}_2/\text{Si}$  substrates are multiplied by a constant of 50 for visual convenience. d) PL spectra of as-grown monolayer  $\text{WS}_2$ , suspended monolayer  $\text{WS}_2$ , and the monolayer  $\text{WS}_2$  transferred onto  $\text{SiO}_2/\text{Si}$  substrates. The spectra of the as-grown and the one on  $\text{SiO}_2/\text{Si}$  substrates are multiplied by 25 and 50, respectively, for visual convenience. Results for monolayer  $\text{WSe}_2$  are given in Figure S1 (Supporting Information).

transferring the synthesized monolayers onto  $\text{SiO}_2/\text{Si}$  substrates prepatterned with holes (Figure 1a,b), which followed a surface-energy-assisted transfer technique that we previously developed (see the Experimental Section).<sup>[6]</sup> Significantly, the suspended monolayers show PL intensities two orders of magnitude ( $\approx 30$ – $60$  times) stronger than the as-grown counterparts under the same incident power (Figure 1c,d; see Figure S1 in the Supporting Information for the result of  $\text{WSe}_2$ ). The incident power used was very small (usually  $< 20 \text{ W cm}^{-2}$ ) to minimize potential heating effect and many body interactions.<sup>[7]</sup> We evaluate the PL efficiency (the number of photons emitted vs the number of photons absorbed) of the monolayers by using Rhodamine 6G dye molecules as a reference (see Figure S1 in the Supporting Information for more details). The typical PL efficiencies are found to be 0.13% and 4.1% for the as-grown and suspended  $\text{MoS}_2$  monolayers, 2.3% and 40% for the as-grown and suspended  $\text{WS}_2$  monolayers, and 0.6% and 22% for the supported and suspended  $\text{WSe}_2$  monolayers, respectively. It is worthwhile to point out that the PL efficiency of the as-grown monolayers varies substantially (by up to one order of magnitude) among different samples or even in the same flake (Figures S2 and S3, Supporting Information) due to the difference in interaction with the substrate and/or in crystalline quality, while the PL of the transferred monolayers is much more uniform (Figure S4, Supporting Information). Without losing generality, the PL efficiency of the as-grown monolayers was obtained from the flakes with relatively high PL intensities, and all the characterizations were performed on the same set of samples if at all possible.

To understand the improved PL efficiency of the suspended monolayers, it is necessary to examine how the transfer process used to prepare the suspended monolayers could impact the materials and the PL. As a matter of fact, the transfer process is very mild with no heat, corrosive chemicals, and capillary forces involved and has been previously demonstrated to be able to preserve the crystalline quality of the monolayers.<sup>[6]</sup>

The preservation of the crystalline quality is also supported by the uniform, strong luminescence at the suspended monolayers (Figure 1b) as well as by a similar width in the Raman peaks of the monolayers before and after the transfer (Figure S5, Supporting Information). Additionally, we confirm that the chemicals involved in the transfer process, including polystyrene, solvent (toluene), and water, may be removed by the mild baking (200–300  $^\circ\text{C}$  under Ar for 30 min) in the transfer process and have only minor effects on the PL (Figure S6, Supporting Information). As further evidence for the minor effect of the transfer process, the monolayer transferred using this wet process shows similar PL efficiency as those transferred by a dry process that involves no chemicals as discussed later (see Figure 3d). Therefore, we can exclude out the transfer process as the reason for the improved PL efficiency in the suspended monolayer.

The substrate is what causes the difference in PL between the supported and suspended monolayers. We find that even a trace amount of moisture at the substrate surface may substantially lower the PL efficiency of  $\text{MoS}_2$  and  $\text{WS}_2$  monolayers by n-doping the monolayers. This is evidenced by one order of magnitude lower PL intensities at the transferred  $\text{MoS}_2$  and  $\text{WS}_2$  monolayers than the as-grown monolayers on the same substrates (Figure 2a,b). The PL of the transferred monolayers is also broader and redshifts compared to those of the as-grown ones. Similar weaker, broader, and redshifted PL can be generally found at the monolayers transferred onto many other substrates including  $\text{SiO}_2/\text{Si}$  (Figure 1), ITO glass, GaN, quartz,  $\text{LaAlO}_3$ ,  $\text{SrTiO}_3$ , and  $\text{SiO}_2/\text{Si}$  functionalized with (3-aminopropyl) trimethoxysilane (Figure S7, Supporting Information). These features indicate that the  $\text{MoS}_2$  and  $\text{WS}_2$  monolayers transferred onto those substrates are heavily n-doped, which has been known to be able to enable trion-dominated emission featuring with lower efficiencies, broader peaks, and longer wavelengths than the exciton emission.<sup>[8]</sup> The n-doping is further supported by the substantial redshift of the  $A_{1g}$  peak, which indicates the concentration of electrons,<sup>[9]</sup> after the monolayer being transferred (Figure S5, Supporting Information). However, the heavy n-doping effect may be only found at the transferred monolayers but not the as-grown and suspended monolayers (Figure 1). It is also absent from the monolayers transferred onto hydrophobic substrates such as Teflon and  $\text{SiO}_2/\text{Si}$  functionalized with octadecyltrichlorosilane (OTS) (Figure 2 and Figure S8, Supporting Information). These strongly suggest that the observed heavy n-doping is contributed by water moisture, more specifically, by the water moisture trapped between the monolayer and the substrate as the water on top of the monolayer can be readily removed during the baking process (Figure S6, Supporting Information). It has been previously demonstrated that the water moisture trapped underneath may strongly n-dope  $\text{MoS}_2$  monolayers.<sup>[10]</sup> As a further evidence to support the adverse effect of water moisture on the PL, we found by exposing the transferred monolayers

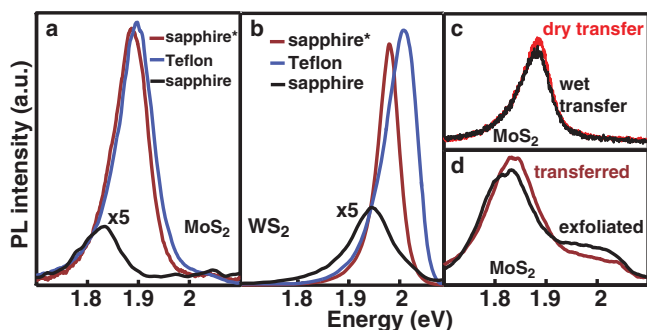


**Figure 2.** Effect of trapped water moisture on the PL efficiency of monolayer  $\text{MoS}_2$  and  $\text{WS}_2$ . a) PL spectra of as-grown monolayer  $\text{MoS}_2$  on sapphire substrates (red curve), the monolayer  $\text{MoS}_2$  transferred onto another sapphire substrate (black curve), and Teflon substrates (blue curve). b) PL spectra of as-grown monolayer  $\text{WS}_2$  on sapphire substrates (red curve), the monolayer  $\text{WS}_2$  transferred onto another sapphire substrate (black curve), and Teflon substrates (blue curve). The PL spectra in (a) and (b) are normalized with respect to the Raman intensity in order to remove the effect of local field enhancements. More specifically, the PL of the monolayers on Teflon substrates is scaled down by a factor of 1.6 due to the local field enhancement caused by the low refractive index of the substrate. c) PL spectra of the monolayer  $\text{MoS}_2$  transferred onto scotch tapes using either the wet process or a dry transfer (directly applying the tape to the as-grown monolayers and then mechanically peeling it off). d) PL spectra of the monolayer  $\text{MoS}_2$  transferred using the wet process and a monolayer  $\text{MoS}_2$  exfoliated from single crystalline bulk materials onto  $\text{SiO}_2/\text{Si}$  substrates.

to concentrated hydrogen sulfuric acid, which has been well known to be able to remove water moisture, may improve the PL to be as good as the as-grown one (Figure S9, Supporting Information). Note that the monolayers transferred onto layered materials substrates such as mica with high hydrophilicity also show no sign of heavy doping, as evidenced by comparable PL in the monolayers transferred and directly grown onto the same layered materials substrates (Figure S10, Supporting Information). This is because the moisture adsorbed onto layered materials substrates, which may bear a less amount of surface defects, is easier to remove during the baking process than those adsorbed onto conventional substrates. We do find a gradual decrease, broadening, and redshift in the PL

of the monolayer transferred onto mica when exposed to an ambient environment as mica may attract moisture from the environment.

The trapped moisture can be mainly correlated to the trace moisture that the substrate intrinsically attracts from the ambient environment, instead of being introduced by the transfer process. Should the water moisture result from the transfer process, we would expect similar heavy n-doping in all the transferred monolayers. The monolayer transferred by using this wet process shows similar PL efficiency to those transferred by a dry process that involves no water (Figure 2c). And the PL of the monolayers transferred on  $\text{SiO}_2/\text{Si}$  substrates using the wet transfer is very similar to the PL of the monolayer mechanically exfoliated from bulk single crystalline onto the same substrates (Figure 2d). It is worthwhile to point out that the PL of our exfoliated monolayers is consistent with the results in references, which often show trion-dominated emission in the mechanically exfoliated  $\text{MoS}_2$  and  $\text{WS}_2$  monolayers on  $\text{SiO}_2/\text{Si}$  substrates.<sup>[2a,c-e, 8a,11]</sup> All these results support that the transfer process is not the main source of the trapped moisture. Very interestingly, the adverse effect of the trapped moisture is negligible for  $\text{WSe}_2$ . The as-grown and transferred monolayer  $\text{WSe}_2$  on  $\text{SiO}_2/\text{Si}$  substrates shows similar PL efficiencies (Figure S1, Supporting Information), which is different from that observed at  $\text{MoS}_2$  and  $\text{WS}_2$  monolayers and indicates much less adverse effect of the trapped water moisture to  $\text{WSe}_2$ . This is due to the different intrinsic doping of these materials as CVD-grown  $\text{MoS}_2$  and  $\text{WS}_2$  monolayers are known intrinsically n-doped while monolayer  $\text{WSe}_2$  intrinsically p-doped.

Except the doping from substrate-borne water moistures, the substrate itself may dope the monolayer and thereby affect the PL. We investigated the PL of the monolayers supported onto a wide variety of substrates where the effect of trapped moistures is minimal. For simplicity, we mainly focus on monolayer  $\text{MoS}_2$ , including as-grown monolayer  $\text{MoS}_2$  on sapphire and the  $\text{MoS}_2$  monolayers transferred onto organic materials or 2D materials substrates. Figure 3a shows the PL of the monolayer  $\text{MoS}_2$  on different substrates (see Figure S8 in the Supporting Information for more results), in which the PL of the suspended  $\text{MoS}_2$  is also given as a reference. Mica substrates may enable

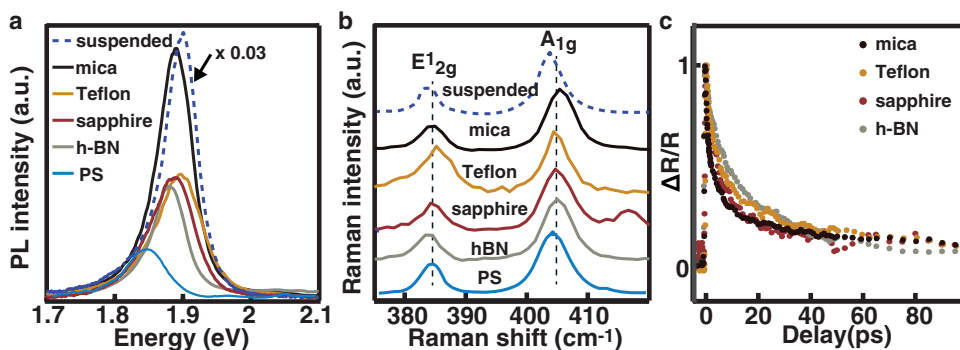


**Figure 3.** Doping effect of the substrate. a) PL spectra of as-grown monolayer  $\text{MoS}_2$  on sapphire substrates (red) and the monolayer transferred onto mica (black), h-BN (gray), and Teflon (orange), and polystyrene (blue) substrates. The PL of suspended monolayer  $\text{MoS}_2$  with the intensity scaled by a factor of 0.03 is also given. The PL of the monolayers on Teflon substrates is scaled down by a factor of 1.6 due to the local field enhancement caused by the low refractive index of the substrate. b) Raman spectra of monolayer  $\text{MoS}_2$  on different substrates. The two dashed lines indicate the  $E_{12g}^1$  and  $A_{1g}$  peaks of the as-grown monolayer. c) Transient differential reflection collected from as-grown monolayer  $\text{MoS}_2$  on sapphire substrates and the monolayer transferred onto mica, Teflon, and h-BN substrates. The measurement for the monolayer on PS is very difficult due to the thermal instability of PS.

**Table 1.** Substrate-induced doping.

	Exciton:trion	Charge transfer <sup>a)</sup>
MoS <sub>2</sub> -Teflon	1:0.120	-0.003
MoS <sub>2</sub> -mica	1:0.08	0.067
MoS <sub>2</sub> -hBN	1:0.11	-0.005
MoS <sub>2</sub> as-grown	1:0.13	-0.003
MoS <sub>2</sub> suspended	1:0.075	N/A
MoS <sub>2</sub> -polystyrene	1:0.213	-0.015

<sup>a)</sup>The amount of electron transfer per MoS<sub>2</sub> unit cell between MoS<sub>2</sub> and the substrate. A positive (negative) value means MoS<sub>2</sub> donates (receives) electron to (from) the substrate.

the strongest PL at the supported monolayer among all the substrates we studied, around two to three times higher than sapphire substrates, while polystyrene substrates are the worst (Figure 3 and Figure S8, Supporting Information). h-BN, which has been reported to be a good substrate for monolayer electronic devices,<sup>[12]</sup> is not as good as mica in terms of promoting the PL in MoS<sub>2</sub>. We can exclude out any substantial effect of strains, which was reported to be able to affect the PL efficiency of monolayers,<sup>[2d,f,8c,13]</sup> in the substrate-dependent PL efficiencies. Only negligible difference (<0.7%) in strain can be found in all the supported and suspended monolayers as indicated by a minor difference in the frequency of the E<sub>2g</sub><sup>1</sup> peak that is known sensitive to strain (Figure 3b and Figure S11, Supporting Information).<sup>[13a,b,14]</sup>

The dependence of the PL efficiencies on substrates as shown in Figure 3a and Figure S8 (Supporting Information) can be mainly ascribed to substrate-induced doping. The higher PL efficiency of the supported monolayer is accompanied with blueshifts of the A<sub>1g</sub> Raman peak, which indicates the decrease of n-doping level (Figure 3b).<sup>[9]</sup> The substrate-induced doping is also supported by the different ratios of trion/exciton emission in the monolayers. We can evaluate the ratio of trion and exciton emissions by numerically fitting the PL spectra (Figure S12, Supporting Information). The fitting result shows that the higher PL efficiency comes with a lower ratio of trion emission (Table 1). For instance, the monolayer on mica substrates shows the lowest ratio of trion emission. Additionally, we simulated the charge transfer between the monolayer and the substrates using density functional theory (DFT) techniques (Figure S13, Supporting Information). The simulation result confirms that mica can provide the best capability to attract electrons (p-doping) from monolayer MoS<sub>2</sub> while polystyrene provides strong n-doping (Table 1). We also studied the PL of monolayer MoS<sub>2</sub> directly grown on substrates including mica, sapphire, GaN, quartz, and SiO<sub>2</sub>/Si (Figures S14 and S15, Supporting Information), in which the effect of trapped moisture can be ignored as well due to the high-temperature treatment of the substrate in the synthetic process. While larger substrate-induced strains (up to 1.4%) could be found in the as-grown monolayers, the main conclusions, including the important role of substrate-induced doping and the best capability of mica to promote the PL efficiency, hold for the as-grown MoS<sub>2</sub> monolayers on different substrates. Similar effect of substrate-induced doping can be found at monolayer WS<sub>2</sub> (Figure S16,

Supporting Information), where the p-doping substrate like mica can best promote the PL. However, the PL in monolayer WSe<sub>2</sub> can be best promoted by the n-doping substrate such as polystyrene and h-BN, and is weaker on p-doping substrates (Figure S17, Supporting Information). Similar to the different effects of water moisture to these materials, this is rooted in the different intrinsic doping of the monolayers, as the CVD-grown WS<sub>2</sub> and MoS<sub>2</sub> are known intrinsically n-doped while the monolayer WSe<sub>2</sub> intrinsically p-doped. The different effects of the same substrate to the monolayers with different intrinsic doping further support the important role of substrate-induced doping in the PL efficiency.

The results given in Figures 2 and 3 indicate that the doping effect of the substrate is far weaker than that of the substrate-borne moisture. This is consistent with previous studies that show strong doping to the monolayers from molecular dopants.<sup>[11a,15]</sup> To better understand the doping effect on the PL efficiency, we investigated the exciton dynamics of the supported monolayers using pump-probing techniques (Figure 3c). What we measured is the differential reflection  $\Delta R/R$  of a delayed probe beam from the monolayers after photoexcitation by a pump beam (590 nm), whose amplitude can be correlated to the concentration of photoexcited charges (see the Experimental Section). While more studies could be necessary, our measurement result nevertheless indicates reasonably similar exciton lifetime with minor variations in all the supported monolayers (Figure 3d). This suggests that the different PL efficiencies caused by the substrate-induced doping may essentially result from different radiative lifetimes; the longer the radiative lifetime, the lower the PL efficiency. A recent study predicts that trions, whose population varies with the doping, indeed have radiative lifetime longer than excitons.<sup>[16]</sup> We would like to point out that the doping from substrates and substrate-borne water moisture, which results from charge transfer, might bear some difference from the doping caused by the implantation or substitution of dopant atoms. In contrast to the substantial shift in the binding energy of Mo atoms observed at Nb-doped MoS<sub>2</sub>,<sup>[17]</sup> we find negligible changes in the binding energy of Mo and S atoms between the as-grown and transferred MoS<sub>2</sub> on sapphire substrates and the monolayer MoS<sub>2</sub> on different substrates (Figure S18, Supporting Information).

The doping effect alone cannot account for the observed dramatic difference in PL efficiencies between the suspended and supported monolayers. In fact, the PL of the suspended MoS<sub>2</sub> monolayer exhibits similar line width and ratio of exciton/trion emission as that of the mica-supported MoS<sub>2</sub> monolayer (Figure 3a and Table 1), suggesting a similar doping level, but its efficiency is more than one order of magnitude higher. We find that, except providing doping to the monolayer, the other significant effect of the substrate is to shorten the exciton lifetime. Figure 4 shows the measured exciton dynamics at the suspended and as-grown monolayers (see the Experimental Section). We have confirmed no substantial heating effect in both suspended and supported monolayers by ensuring a linear dependence of the  $\Delta R/R$  at the zero second delay on the pumping fluence (Figure S19, Supporting Information). Upon photoexcitation,  $\Delta R/R$  arises to its maximum value within  $\approx 500$  fs for all the monolayers (Figure 4), which is consistent with that previously reported.<sup>[2j,18]</sup> However, the decay of

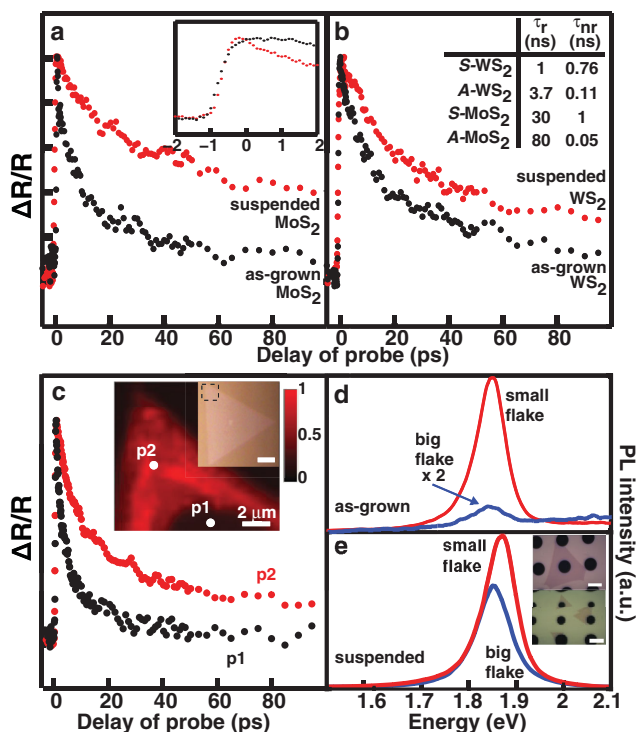


**Figure 4.** Effect of the substrate on exciton dynamics. The transient differential reflection measured from a) suspended and as-grown MoS<sub>2</sub> monolayers and b) suspended and as-grown WS<sub>2</sub> monolayers. The inset of (a) is to illustrate the result around the zero-picosecond decay, and the inset of (b) lists the radiative and non-radiative lifetimes of suspended WS<sub>2</sub> (S-WS<sub>2</sub>), as-grown WS<sub>2</sub> (A-WS<sub>2</sub>) on sapphire substrates, suspended MoS<sub>2</sub> (S-MoS<sub>2</sub>), and as-grown MoS<sub>2</sub> (A-MoS<sub>2</sub>) on sapphire substrates. c) The transient differential reflection collected from two different areas p1 and p2 on one single flake as indicated. The p1 is from the central area with low PL while the p2 from the edge area with high PL as indicated in the PL mapping. Inset: PL mapping and optical image of the flake in which the dashed square indicates where the mapping PL was collected from (scale bar, 10 μm). The PL spectra collected from d) the as-grown and e) suspended flakes with different sizes (≈50 and ≈8 μm). The inset of (e) shows the optical image of the suspended flakes.

the charge carriers in the suspended monolayers is obviously slower than that in the supported monolayers. This dynamics process is more complicated than that previously reported,<sup>[2],19]</sup> involving exciton–exciton annihilations. We have performed thorough analysis on the exciton dynamics, the details of which are given in a separate paper.<sup>[7]</sup> Our analysis indicates that the suspension may cause the exciton lifetime to increase by around seven times (from 110 to 760 ps) for monolayer WS<sub>2</sub> and around 20 times (from 50 to 1 ns) for monolayer MoS<sub>2</sub>. We have also confirmed the exciton recombination in the supported MoS<sub>2</sub> monolayers is dominated by a defect-assisted mechanism as evidenced by independence of the dynamics on pumping fluence and temperature (Figure S19–S20, Supporting Information), which is consistent with that previously reported.<sup>[19,20]</sup> The substantial larger exciton lifetime at the suspended monolayers indicates that the substrate may facilitate the defect-assisted nonradiative recombination.

The effect of the substrate on the defect-assisted recombination is dependent on the crystalline quality of the monolayer, in particular, sulfur vacancies. We observed the PL at the edge

stronger than the center area of as-grown WS<sub>2</sub> monolayer (Figure 4c) and also the PL at smaller monolayer flakes much stronger than at bigger counterparts (Figure 4d), even though the doping levels are similar as indicated by identical PL wavelengths (Figure S21, Supporting Information). The lower PL is often accompanied with a shorter exciton lifetime, indicating faster defect-assisted exciton recombination (Figure 4c). According to previous studies,<sup>[21]</sup> this PL nonuniformity can be correlated to different concentrations of sulfur vacancies as the center area or larger flakes may bear more sulfur vacancies due to the longer exposure to the high temperature growth environment. However, regardless the huge difference in the PL of as-grown monolayers, the PL efficiency and exciton dynamics of suspended monolayers always show to be similar with only minor variation (Figure 4e and Figure S22, Supporting Information). This suggests that the defect-assisted nonradiative recombination in the supported monolayers depends on the interaction of the defects in the monolayer with the substrate. The defects might provide a channel for the substrate to affect the exciton dynamics. Our results suggest that the nonradiative recombination may be suppressed by decreasing the number of defects. The observed bigger increase in the exciton lifetime of monolayer MoS<sub>2</sub> than WS<sub>2</sub> after being suspended (Figure 4a,b) may be ascribed to the higher crystalline quality of monolayer WS<sub>2</sub>, as it has generally been believed that monolayer WS<sub>2</sub> may have less defects than monolayer MoS<sub>2</sub>.

As the last note, we examine the effect of the dielectric environment created by the substrate on the PL of the monolayer. The dielectric environment may have effect on the local electromagnetic field due to the multiple reflection inside the monolayer as illustrated in Figure 5a. This is evidenced by stronger Raman intensities of the suspended monolayers, approximately four to five times stronger than that of the supported counterparts (Figure 5b,c and Figure S23, Supporting Information). The enhancement  $Q_{\text{field}}$  of the local field at the suspended monolayer with respect to the supported counterpart can be derived from the Raman enhancement  $Q_{\text{Ram}}$  as  $Q_{\text{field}} = (Q_{\text{Ram}})^{0.5}$ , which is estimated to be around 2–2.2 based on the Raman measurement. This is consistent with our calculation using the refractive index we measured<sup>[22]</sup> (Figure S24, Supporting Information) and a well-established analytical model (see Figure S2 in the Supporting Information). The local field enhancement  $Q_{\text{field}}$  can lead to an increase in the radiative decay (or decrease in radiative lifetime) of the suspended monolayers. The dielectric environment may also affect the radiative lifetime by providing dielectric screening to change exciton binding energy. Our previous analysis indicates suspending the monolayer may decrease the radiative lifetime by around 2.7–4 times (from 3.7 to 1 ns for WS<sub>2</sub> and 80 to 30 ns for MoS<sub>2</sub>).<sup>[7]</sup> Given the expected decrease of radiative lifetime (by 2–2.2 times) due to the local field enhancement, the effect of the increase of exciton binding energy on the PL efficiency is estimated by a factor no more than 1.4–1.8.

### 3. Conclusions

In conclusion, we demonstrate that substrates can significantly limit the PL efficiency of monolayer TMDC materials, mainly

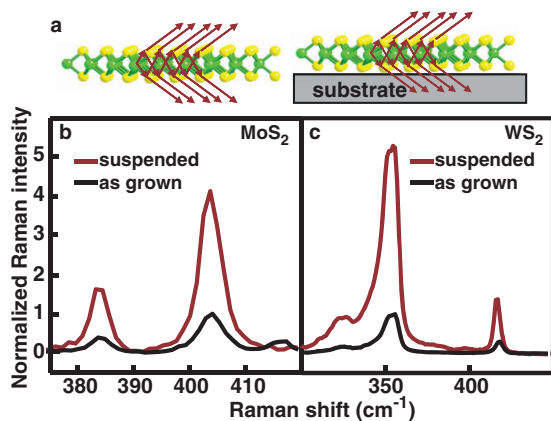


**Figure 5.** Effect of the substrate on radiative decay. a) Schematic illustration for the interference of radiated light in the monolayers without and with the presence of substrates. Raman spectra of b) suspended and as-grown MoS<sub>2</sub> monolayers and c) suspended and as-grown WS<sub>2</sub> monolayers. See Figure S23 in the Supporting Information for the result of WSe<sub>2</sub>.

through doping the monolayer and facilitating defect-assisted nonradiative exciton recombinations. The doping may be from substrate-borne moisture and the substrate, the former of which is much stronger than the latter for monolayer MoS<sub>2</sub> and WS<sub>2</sub> but typically negligible for monolayer WSe<sub>2</sub>. The doping effect can be substantially mitigated by using proper substrates, more specifically, p-doping substrates like mica for monolayer WS<sub>2</sub> and MoS<sub>2</sub> and n-doping substrates like h-BN and polystyrene for monolayer WSe<sub>2</sub>. The defect-assisted recombination depends on the interaction between the defects such as sulfur vacancies in the monolayers and the substrate, and can be suppressed by either removing the substrates or lowering the number of defects. The result may provide very useful guidance for the rational design of high-performance 2D TMDC materials light emission devices. It indicates that organic materials or 2D materials may generally make good substrates for the device development with the monolayers, and that WSe<sub>2</sub> may provide a better platform than MoS<sub>2</sub> and WS<sub>2</sub> due to its less sensitivity to water moisture. Additionally, it indicates that a key strategy to improve the light emission efficiency is eliminating the defect–substrate interaction by either decreasing the number of defects or removing the substrate.

#### 4. Experimental Section

**Synthesis and Transfer of MoS<sub>2</sub> and WS<sub>2</sub> Monolayers:** The monolayers were grown using a CVD reported previously.<sup>[5]</sup> Typically, sulfur powder (Sigma-Aldrich) and MoO<sub>3</sub> (WO<sub>3</sub>) (99.99%, Sigma-Aldrich) source material were placed in the upstream and the center of a tube furnace, respectively. And substrates (usually sapphire) were placed at the downstream of the tube. Typical growth was performed at 750 °C (900 °C) for 10 (30) min under a flow of Ar gas in rate of 100 sccm and ambient pressure.

The transfer of the monolayers followed a surface-energy-assisted transfer approach that we have developed previously.<sup>[6]</sup> In a typical transfer process, 9 g of PS with a molecular weight of 280 000 g mol<sup>-1</sup> was dissolved in toluene (100 mL), and then the PS solution was spin-coated (3000 rpm for 60 s) on the as-grown monolayers. This was followed by a baking at 80–90 °C for 1 h. A water droplet was then

dropped on top of the monolayer. Due to the different surface energies of the monolayer and the substrate, water molecules could penetrate under the monolayer, resulting in the delamination of the PS-monolayer assembly. The polymer/monolayer assembly could be picked up with a tweezers and was transferred to different substrates. After that, the transferred PS-monolayer assembly was baked at 80 °C for 1 h and a final baking was performed for 30 min at 150 °C. Finally, PS was removed by rinsing with toluene several times.

**Characterizations:** Raman and PL mapping were carried out by Horiba Labram HR800 system with a 532 nm laser. All other Raman spectra were collected on a Renishaw-1000 Raman spectroscopy with an excitation wavelength of 514.5 nm. A home-built setup that consists of a confocal microscope (Nikon Eclipse C1) connected with a monochromator (SpectraPro, Princeton Instruments) and a detector (Pixis, Princeton Instruments) was used to perform the photoluminescence measurement with an excitation wavelength of 532 nm. Shimadzu UV-3600 UV-VIS-NIR Spectrophotometer and Edinburgh FL/FS920 Spectrometer were used to measure the absorption and photoluminescence of rhodamine-6g doped PMMA film and rhodamine-6g solution (300 × 10<sup>-6</sup> M in methanol).

A 150 fs pulse at 2.10 eV is used to pump electrons from the valence band into conduction band of the monolayers. The differential reflection ( $\Delta R/R$ ) of a time-delayed pulse, whose wavelength is chosen to match the A exciton ( $\approx 1.88$  eV for MoS<sub>2</sub> and 2 eV for WS<sub>2</sub>, respectively), was used to probe the monolayers after the photoexcitation. The pumping and probe beams were collinearly polarized before entering into a 50X long working distance objective and the reflected probe pulse was collected using the same objective. A monochromator and a Si photodetector combination measured the differential reflection using lock-in amplifications. Typical pumping fluence used in the experiment was less than 10  $\mu\text{J cm}^{-2}$ . Unless otherwise specified, all experiments were performed at room temperature.

**DFT Computation:** The first-principles calculations were performed by using Vienna ab initio simulation package (VASP) within the framework of density functional theory. Van der Waals corrected functional with Becke88 optimization (optB88) was adopted to consider the dispersive interaction between the MoS<sub>2</sub> and the substrate. A kinetic energy cutoff of 400 eV of the plane wave basis was used. A criterion was used for the *k*-point sampling based on Monkhorst-Pack grid such that the number of the *k* points along the inplane periodic direction was determined by the smallest integer that fulfills  $n_k L = 60 \text{ \AA}$ , where *L* is the lattice constant of the supercell in the periodic direction. The various substrates supported MoS<sub>2</sub> systems were simulated by creating slab models and supercells were created by considering the lattice commensuration between each type of substrate and the MoS<sub>2</sub> layer. A vacuum layer with thickness greater than 15 Å was adopted to avoid the spurious interaction due to the periodic image and dipole corrections were implemented to consider the asymmetry of the slabs. The structures were relaxed until the forces on each atom are less than 0.005 eV Å<sup>-1</sup>. To analyze the charge dynamics across the MoS<sub>2</sub>–substrate interface, the differential charge density (DCD)  $\Delta\rho(r)$  and the plane-averaged DCD  $\Delta\rho(z)$  along the direction normal to the interface were calculated by integrating DCD within the *x*–*y* plane. The amount of transferred charge at the *z* point from the bottom layer was obtained according to  $\Delta Q(z) = \int_{-\infty}^z \Delta\rho(z') dz'$

#### Supporting Information

Supporting Information is available from the Wiley Online Library or from the author.

#### Acknowledgements

Y.Y., Y.Y., and C.X. contributed equally to this work. This work was supported by a CAREER award from the National Science Foundation (DMR-1352028). Y. Zhang (UNCC) acknowledges the support of Bissell

Distinguished Professorship. The authors thank F. Castellano for help with the measurement of PL and absorption of R6G solution and films, and thank E. Keenan and Y. Wei for providing SiO<sub>2</sub>/Si substrates functionalized with self-assembled monolayers of OTS. Y. Q. Cai and Y. W. Zhang are grateful for the support from the Agency for Science, Technology and Research (A\*STAR) and the computational resource provided by A\*STAR Computational Resource Centre, Singapore (ACRC). The authors acknowledge the use of the Analytical Instrumentation Facility (AIF) at North Carolina State University, which is supported by the State of North Carolina and the National Science Foundation. The authors declare no competing financial interests.

Received: January 25, 2016

Revised: March 11, 2016

Published online: May 6, 2016

- [1] a) L. Y. Cao, *MRS Bull.* **2015**, *40*, 592; b) Q. H. Wang, K. Kalantar-Zadeh, A. Kis, J. N. Coleman, M. S. Strano, *Nat. Nanotechnol.* **2012**, *7*, 699.
- [2] a) M. Buscema, G. A. Steele, H. S. van der Zant, A. Castellanos-Gomez, *Nano Res.* **2014**, *7*, 561; b) W. C. Jin, P. C. Yeh, N. Zaki, D. T. Zhang, J. T. Liou, J. T. Sadowski, A. Barinov, M. Yablonskikh, J. I. Dadap, P. Sutter, I. P. Herman, R. M. Osgood, *Phys. Rev. B* **2015**, *91*, 121409; c) K. F. Mak, C. Lee, J. Hone, J. Shan, T. F. Heinz, *Phys. Rev. Lett.* **2010**, *105*, 136805; d) N. Scheuschner, O. Ochedowski, A.-M. Kaulitz, R. Gillen, M. Schleberger, J. Maultzsch, *Phys. Rev. B* **2014**, *89*, 125406; e) D. Sercombe, S. Schwarz, O. Del Pozo-Zamudio, F. Liu, B. Robinson, E. Chekhovich, I. Tartakovskii, O. Kolosov, A. Tartakovskii, *Sci. Rep.* **2013**, *3*, 3489; f) Z. Liu, M. Amani, S. Najmaei, Q. Xu, X. Zou, W. Zhou, T. Yu, C. Qiu, A. G. Birdwell, F. J. Crowne, R. Vajtai, B. I. Yakobson, Z. Xia, M. Dubey, P. M. Ajayan, J. Lou, *Nat. Commun.* **2014**, *5*, 5246; g) M. M. Ugeda, A. J. Bradley, S.-F. Shi, F. H. d. Jornada, Y. Zhang, D. Y. Qiu, W. Ruan, S.-K. Mo, Z. Hussain, Z.-X. Shen, F. Wang, S. G. Louie, M. F. Crommie, *Nat. Mater.* **2014**, *13*, 1091; h) L. Su, Y. Yu, L. Cao, Y. Zhang, *Nano Res.* **2015**, *8*, 2686; i) S. Najmaei, X. Zou, D. Er, J. Li, Z. Jin, W. Gao, Q. Zhang, S. Park, L. Ge, S. Lei, *Nano Lett.* **2014**, *14*, 1354; j) H. Shi, R. Yan, S. Bertolazzi, J. Brivio, B. Gao, A. Kis, D. Jena, H. G. Xing, L. Huang, *ACS Nano* **2013**, *7*, 1072; k) M. Palummo, M. Bernardi, J. C. Grossman, *Nano Lett.* **2015**, *15*, 2794.
- [3] Y. Lin, X. Ling, L. Yu, S. Huang, A. L. Hsu, Y.-H. Lee, J. Kong, M. S. Dresselhaus, T. Palacios, *Nano Lett.* **2014**, *14*, 5569.
- [4] D.-H. Lien, J. S. Kang, M. Amani, K. Chen, M. Tosun, H.-P. Wang, T. Roy, M. S. Eggleston, M. C. Wu, M. Dubey, *Nano Lett.* **2015**, *15*, 1356.
- [5] Y. Yu, S. Hu, L. Su, L. Huang, Y. Liu, Z. Jin, A. A. Purezky, D. B. Geohegan, K. W. Kim, Y. Zhang, *Nano Lett.* **2014**, *15*, 486.
- [6] A. Gurarlan, Y. Yu, L. Su, Y. Yu, F. Suarez, S. Yao, Y. Zhu, M. Ozturk, Y. Zhang, L. Cao, *ACS Nano* **2014**, *8*, 11522.
- [7] Y. Yu, Y. Yu, C. Wang, K. Gundogdu, L. Cao, **2015**, DOI: arXiv:1512.00945.
- [8] a) K. F. Mak, K. L. He, C. Lee, G. H. Lee, J. Hone, T. F. Heinz, J. Shan, *Nat. Mater.* **2013**, *12*, 207; b) B. R. Zhu, X. Chen, X. D. Cui, *Sci. Rep.* **2015**, *5*, 9218; c) J. S. Ross, S. Wu, H. Yu, N. J. Ghimire, A. M. Jones, G. Aivazian, J. Yan, D. G. Mandrus, D. Xiao, W. Yao, X. Xu, *Nat. Commun.* **2013**, *4*, 1474.
- [9] B. Chakraborty, A. Bera, D. V. S. Muthu, S. Bhowmick, U. V. Waghmare, A. K. Sood, *Phys. Rev. B* **2012**, *85*, 161403(R).
- [10] a) J. O. Varghese, P. Agbo, A. M. Sutherland, V. W. Brar, G. R. Rossman, H. B. Gray, J. R. Heath, *Adv. Mater.* **2015**, *27*, 2734; b) C. X. Zheng, Z. Q. Xu, Q. H. Zhang, M. T. Edmonds, K. Watanabe, T. Taniguchi, Q. L. Bao, M. S. Fuhrer, *Nano Lett.* **2015**, *15*, 3096.
- [11] a) N. Peimyoo, W. Yang, J. Shang, X. Shen, Y. Wang, T. Yu, *ACS Nano* **2014**, *8*, 11320; b) H. Nan, Z. Wang, W. Wang, Z. Liang, Y. Lu, Q. Chen, D. He, P. Tan, F. Miao, X. Wang, J. Wang, Z. Ni, *ACS Nano* **2014**, *8*, 5738.
- [12] G.-H. Lee, Y.-J. Yu, X. Cui, N. Petrone, C.-H. Lee, M. S. Choi, D.-Y. Lee, C. Lee, W. J. Yoo, K. Watanabe, *ACS Nano* **2013**, *7*, 7931.
- [13] a) A. Castellanos-Gomez, R. Roldán, E. Cappelluti, M. Buscema, F. Guinea, H. S. van der Zant, G. A. Steele, *Nano Lett.* **2013**, *13*, 5361; b) H. J. Conley, B. Wang, J. I. Ziegler, R. F. Haglund Jr., S. T. Pantelides, K. I. Bolotin, *Nano Lett.* **2013**, *13*, 3626; c) S. B. Desai, G. Seo, J. S. Kang, H. Fang, C. Battaglia, R. Kapadia, J. W. Ager, J. Guo, A. Javey, *Nano Lett.* **2014**, *14*, 4592; d) J. Feng, X. F. Qian, C. W. Huang, J. Li, *Nat. Photon.* **2012**, *6*, 865; e) H. Li, A. W. Contryman, X. Qian, S. M. Ardakani, Y. Gong, X. Wang, J. M. Weisse, C. H. Lee, J. Zhao, P. M. Ajayan, J. Li, H. C. Manoharan, X. Zheng, *Nat. Commun.* **2015**, *6*, 7381.
- [14] C. Rice, R. Young, R. Zan, U. Bangert, D. Wolverson, T. Georgiou, R. Jalil, K. Novoselov, *Phys. Rev. B* **2013**, *87*, 081307.
- [15] a) S. Mouri, Y. Miyauchi, K. Matsuda, *Nano Lett.* **2013**, *13*, 5944; b) S. Tongay, J. Zhou, C. Ataca, J. Liu, J. S. Kang, T. S. Matthews, L. You, J. B. Li, J. C. Grossman, J. Q. Wu, *Nano Lett.* **2013**, *13*, 2831.
- [16] H. Wang, C. Zhang, W. Chan, C. Manolatu, S. Tiwari, F. Rana, *Phys. Rev. B* **2016**, *93*, 045407.
- [17] J. Suh, T. E. Park, D. Y. Lin, D. Y. Fu, J. Park, H. J. Jung, Y. B. Chen, C. Ko, C. Jang, Y. H. Sun, R. Sinclair, J. Chang, S. Tongay, J. Q. Wu, *Nano Lett.* **2014**, *14*, 6976; b) A. Nipane, D. Karmakar, N. Kaushik, S. Karande, S. Lodha, *ACS Nano* **2016**, *10*, 2128.
- [18] Z. Nie, R. Long, L. Sun, C.-C. Huang, J. Zhang, Q. Xiong, D. W. Hewak, Z. Shen, O. V. Prezhdo, Z.-H. Loh, *ACS Nano* **2014**, *8*, 10931.
- [19] H. Wang, C. Zhang, F. Rana, *Nano Lett.* **2015**, *15*, 339.
- [20] C. J. Docherty, P. Parkinson, H. J. Joyce, M.-H. Chiu, C.-H. Chen, M.-Y. Lee, L.-J. Li, L. M. Herz, M. B. Johnston, *ACS Nano* **2014**, *8*, 11147.
- [21] a) C. Cong, J. Shang, X. Wu, B. Cao, N. Peimyoo, C. Qiu, L. Sun, T. Yu, *Adv. Opt. Mater.* **2014**, *2*, 131; b) N. Peimyoo, J. Shang, C. Cong, X. Shen, X. Wu, E. K. L. Yeow, T. Yu, *ACS Nano* **2013**, *12*, 10985.
- [22] Y. Yu, Y. Yu, Y. Cai, W. Li, A. Gurarlan, H. Peelaers, D. E. Aspnes, C. G. V. d. Walle, N. V. Nguyen, Y.-W. Zhang, L. Cao, *Sci. Rep.* **2015**, *5*, 16996.